Received: 9 May 2024 | Revised: 22 July 2024 | Accepted: 23 July 2024

DOI: 10.1096/fba.2024-00070

RESEARCH ARTICLE

FASEB BioAdvances WILEY

Insights on pathophysiology of hydrocephalus rats induced by kaolin injection

Kuo Zhang[1,2,3] | **Wanqi Zhou**[1] | **Huijie Yu**[4] | **Meijun Pang**[1,2,3] | **Huixin Gao**[1] | **Faheem Anwar**[1] | **Kai Yu**[4] | **Ziwei Zhou**[4] | **Fang Guo**[5] | **Xiuyun Liu**[1,2,3,6] | **Dong Ming**[1,2,3]

[1]Academy of Medical Engineering and Translational Medicine, Tianjin University, Tianjin, China

[2]State Key Laboratory of Advanced Medical Materials and Devices, Medical School, Tianjin University, Tianjin, China

[3]Haihe Laboratory of Brain-Computer Interaction and Human-Machine Integration, Tianjin, China

[4]Tianjin General Hospital, Tianjin Medical University, Tianjin, China

[5]Tianjin Huanhu Hospital, Tianjin, China

[6]School of Pharmaceutical Science and Technology, Tianjin University, Tianjin, China

Correspondence
Xiuyun Liu and Dong Ming, Academy of Medical Engineering and Translational Medicine, Tianjin University, Tianjin, 300072, China.
Email: xiuyun_liu@tju.edu.cn and richardming@tju.edu.cn

Abstract

Hydrocephalus can affect brain function and motor ability. Current treatments mostly involve invasive surgeries, with a high risk of postoperative infections and failure. A successful animal model plays a significant role in developing new treatments for hydrocephalus. Hydrocephalus was induced in Sprague–Dawley rats by injecting 25% kaolin into the subarachnoid space at the cerebral convexities with different volumes of 30, 60 and 90 μL. Magnetic resonance imaging (MRI) was performed 1 month and 4 months after kaolin injection. The behavioral performance was assessed weekly, lasting for 7 weeks. The histopathological analyses were conducted to the lateral ventricles by hematoxylin–eosin (HE) staining. Transcriptomic analysis was used between Normal Pressure Hydrocephalus (NPH) patients and hydrocephalus rats. MRI showed a progressive enlargement of ventricles in hydrocephalus group. Kaolin-60 μL and kaolin-90 μL groups showed larger ventricular size, higher anxiety level, bigger decline in body weight, motor ability and cognitive competence. These symptoms may be due to higher-grade inflammatory infiltrate and the damage of the structure of ependymal layer of the ventricles, indicated by HE staining. The overlap upregulated genes and pathways mainly involve immunity and inflammation. Transcriptomic revealed shared pathogenic genes CD40, CD44, CXCL10, and ICAM1 playing a dominance role. 60 μL injection might be recommended for the establishment of hydrocephalus animal model, with a high successful rate and high stability. The hydrocephalus model was able to resemble the inflammatory mechanism and

Abbreviations: CC, cellular component; DEGs, differentially expressed genes; GEO, Gene Expression Omnibus; GO, Gene Ontology; HE, hematoxylin–eosin; IVH, intraventricular hemorrhage; KEGG, Kyoto Encyclopedia of Genes and Genomes; MRI, magnetic resonance imaging; NF-κB, Nuclear factor kappa B; NPH, normal pressure hydrocephalus; PC1, first principal component; PC2, second principal component; PCA, principal component analysis; PHH, post-hemorrhagic hydrocephalus; PIH, infectious hydrocephalus; RNA-seq, RNA sequencing; SD, Standard deviations; TLR4, Toll-like receptor 4; VST, variance-stabilized transformation.

Kuo Zhang and Wanqi Zhou share the same first authorship.

Xiuyun Liu and Dong Ming share the same senior authorship.

behavioral performance observed in human NPH patients, providing insights for identifying therapeutic targets for hydrocephalus.

KEYWORDS

animal model, brain imaging, hydrocephalus, inflammation, kaolin injection, subarachnoid space, transcriptome

1 | INTRODUCTION

Hydrocephalus is characterized by enlarged ventricle, caused by excessive cerebral spinal fluid in the ventricles due to the blockage of CSF absorption or excessive CSF secretion.[1] It often happens in children (≤18 years) and the elderly (≥65 years), with a prevalence of 88/100,000 and 175/100,000, respectively. Moreover, the prevalence is higher in middle- and low-income countries compared to high-income countries.[2] Hydrocephalus is a chronic disease,[3] which causes many complications including seizures, developmental delays, motor impairment, dementia, and gait difficulties.[4] If left untreated, it may lead to progressive nerve damage and influence patients life quality.[5] The current treatment for hydrocephalus mostly involves surgeries, such as insertion of a shunt, endoscopic third ventriculostomy, which carry a high risk of infection and failure.[6,7] A successful animal model will play a significant role in developing innovative treatments for hydrocephalus.

Several animal hydrocephalic models have been developed in the past several decades. Davis et al.[8] introduced hydrocephalus in newborn hamsters and cats through intracerebral viral inoculation. Fiori et al.[9] investigated the effect of using neurotoxins such as single intraperitoneal injection of β, β′-iminodipropionitrile in inducing hydrocephalus. Moinuddin and Tada[10] studied CSF flow dynamics in transforming growth factor beta 1-induced chronic hydrocephalus mice. Wiesmann et al.[11] performed bacterial inoculations to induce hydrocephalus, which may also cause diseases such as meningitis affecting the study of hydrocephalus. Borit and Sidman[12] created a new mouse model with communicating hydrocephalus by carrying the tumbler mutation. Dahme et al.[13] discovered that disrupting the L1 gene in mice led to hydrocephalus, which contributed to clarifying how genetic influences impact the functions of L1 in the nervous system.

Another widely used animal model for hydrocephalus is kaolin injection which was first introduce by Dixon in 1932, with a big advantage of inducing minimal injury to the distal structures.[14,15] Two widely used locations for kaolin injection include basal cistern and cisterna magna to induce subacute hydrocephalus.[16,17] Other locations have also been tried to simulate the chronic hydrocephalus or normal pressure hydrocephalus (NPH).[18,19] Li et al.[19] attempted to inject kaolin in the convex subarachnoid space of the cerebral cortex through bilateral craniotomy with a low success rate of 31%. Later, Jusué-Torres et al.[18] improved this model by thinning the parietal bone rather than removing it; however, the ideal injection volume of kaolin has not been determined. Besides the issues mentioned above, current animal models still need further improvement and validation via behavior test, brain imaging, and other techniques. A precise volume also needs to be clarified to standardize the procedure of introducing a hydrocephalus animal model with kaolin injection into the subarachnoid space.

The current study aims to comprehensively expand the characterization of brain damage in hydrocephalus rats induced by kaolin injection into the subarachnoid space and to understand how the model mimics NPH by transcriptomic analysis. We wish to provide a standard strategy for establishing a hydrocephalus model and to gain a deeper understanding of the model's clinical relevance to NPH patients for future research.

2 | MATERIALS AND METHODS

2.1 | Animals

Twenty-four adult female Sprague Dawley rats (220 g ± 20 g), which were 2 months old, were purchased from Beijing Vitonlivar Laboratory Animal Technology Co (No. SCXK 2021–0006, Beijing, China). The rats experienced a 1-week acclimatization period before the start of the experiment. During the experiment, all rats were housed in a 12-h light–dark cycle environment and have free access to food and water. All the procedures followed the U.K. Animals (Scientific Procedures) Act, 1986 and associated guidelines, the U.S. National Research Council's Guide for the Care and Use of Laboratory Animals and were approved by the Animal Ethics Committee of Tianjin University in China (No. TJUE-2023-070). The rats were randomly divided into four groups with six rats in each group: intact controls; three hydrocephalus model groups

with kaolin injections of 30, 60 and 90 μL, label as kaolin-30 μL, kaolin-60 μL and kaolin-90 μL respectively.

2.2 | Hydrocephalus induction

A gas mask was attached to provide continuous anesthesia during the whole procedure, with 3% isoflurane. The heart rate was monitored to allow for timely adjustment of anesthetic parameters. The rats were shaved and then coated with depilatory cream for 5 min. The depilatory cream was wiped off with cotton balls dipped in warm water afterwards. A midline incision was made on the skin of the head, and the drilling sites were marked between the coronal and lambdoid sutures.

A surgical drill was used to thin the skull until it can be easily penetrated with a microsampler (diameter: 0.5 mm, scale: 100 μL, Shanghai High Pigeon Industry & Trade Co). A 25% sterile kaolin suspension prepared in saline was injected into the subarachnoid space of bilateral cerebral convexities with 30, 60, or 90 μL at the speed of approximately 2 μL/s (Figure S1). The injection site was pressed with a cotton ball for half a minute. The bone hole was sealed with bone wax. Then, the skin incision was closed with a fhx3-0 suture and dabbed it with glue. Chitosan gel was used to combat bacteria and promote wound healing which was applied before anesthesia recovery. Chitosan spray was used on the wound for the next 3 days.

2.3 | Behavioral tests

Behavioral tests were conducted weekly, lasting for 7 weeks after kaolin injection, including open field test, new object recognition and Y-maze. At the end of each test, 75% alcohol was used to clean the equipment and then wiped with water (Figure 1).

2.3.1 | Motor ability and anxiety level test

Open field test was used to study the spontaneous exploratory behavior of animals in a square arena. The total open field is 100 × 100 × 40 cm, the center arena is defined as 50 × 50 cm. Rats were placed in the center of the open field and allowed to explore freely for 5 min. The total distance was used to assess motor ability and the entries in the center area was used to assess anxiety level.

2.3.2 | Recognition test

Novel object recognition test was used to study cognitive memory levels of the animals. Rats were placed in the same field as described before. During the training period, two identical objects were placed in a central symmetrical position of the area and the rats were given a train session for 10 min. When all rats had completed the training, one of the objects was replaced with a new one and the rats were given a 5-min test. The recognition index was computed as the percentage of time spent exploring the new object over the total time spent exploring the two objects.[20]

The Y-maze spontaneous alternation experiment was used to test the spatial recognition abilities of rats. The Y-maze consists of three identical arms, each with an angle of 120° between them. The size of each arm is 500 × 100 × 300 mm. The rats were placed in the same position each time and were allowed to explore the surrounding area freely for 5 min. Spatial recognition ability is measured by the rate of spontaneous alternation, which is calculated as (Total alternations/Total arms entered-2) × 100%, with total alternations referring to the number of three consecutive entries in different arms.[21] The test procedures of the above three experiments were recorded by a Sony video camera, and the trace analysis of the rats was recorded using SMART 3.0 video tracking

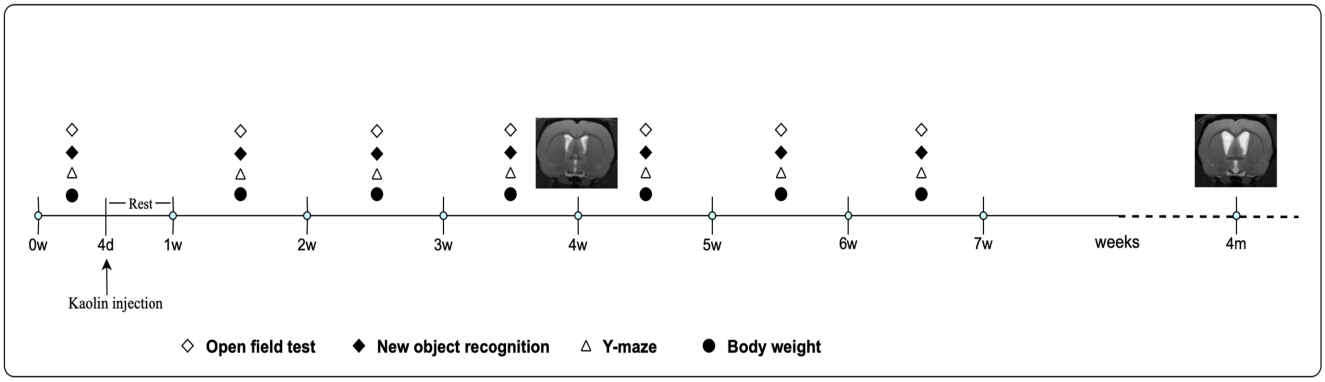

FIGURE 1 The details of the experimental procedures. Kaolin was injected on the 4th day. Behavioral tests and body weight assessment were conducted weekly, lasting for 7 weeks. MRI was performed 1 month and 4 months after kaolin injection. Hollow diamond: Open field test, solid diamond: New object recognition, triangle: Y-maze, circle: Body weight.

software (Panlab Harvard Apparatus, Inc., Holliston, MA, USA).

2.4 | Body weight

Significant loss of body weight was an important indicator of the success of hydrocephalus model establishment.[15] Therefore, the weight of the animals was recorded weekly before kaolin injection until 7 weeks after kaolin injection.

2.5 | Magnetic resonance imaging (MRI)

MRI was conducted in the first and fourth months after kaolin injection, at the Multimodality Preclinical Molecular Imaging Center, General Hospital of Tianjin Medical University using a Bruker BioSpec 9.4 T small animal scanner (with 900mT/m maximum gradient strength, and 4200 T/m/s slew rate, Bruker Corporation, Billerica, Massachusetts). After anesthesia with 3.5% isoflurane, rats were placed in a 30 cm volume super-shielded superconducting magnet for transmission. T2-weight images of coronal were obtained with a 3.6 cm × 3.6 cm field-of-view (35 slices, 0.8-mm slice thickness, 33-ms echo time, 2802.49-ms repetition time, relaxation enhancement factor of eight, number of averages of two). The matrix size was 256 mm × 256 mm, and the in-plane resolution was 0.141 mm × 0.141 mm.

The Evans Index was used to assess the extent of lateral ventricular enlargement by T2-weighted images at the level of the anterior commissure. The Evans index was calculated as the ratio of the maximum width of the anterior horn of the lateral ventricle to the maximum width of the cranial cavity within the same dimension.[18] Evans index over 0.3 is considered a hydrocephalus state.

2.6 | Histological studies

After administering gas anesthesia with Isoflurane, the rats were given a lethal dose of pentobarbital.[15] Perform heart perfusion while the heart is still beating, using phosphate buffered saline with a perfusion pump (LongerPump®, BT100-3J) for 10 min, followed by 4% paraformaldehyde perfusion for 8 min. After skull removal, the brain tissue was immersed in polyformaldehyde at 4°C for 24 h. Subsequently, it underwent cryoprotection using sucrose gradients with concentrations of 15% and 30% in turn, until the brain tissue sank. The brain was then embedded in optimal cutting temperature compound and stored in an ultra-freezer at −80°C. The samples were cut in a coronal plane using a cryostat in sections 15 μm thick and mounted onto adhesion microscope slides. The slides at the level of the lateral ventricles were then subjected for hematoxylin–eosin (HE) staining.[22]

First, the slides were staining by immersing them in hematoxylin solution to stain the nuclei. Then, the slides were rinsed with water. Differentiation solution was used to remove excess hematoxylin and control the intensity of staining. Subsequently, the slides were rinsed in running water for blueing the nuclei and then submerged in eosin solution to stain the cytoplasm and extracellular components. To complete the process, the slides underwent dehydration using a series of increasing alcohol concentrations, followed by clearing with xylene to rendering them transparent. Finally, the sections were covered with a coverslip using neutral mounting medium.

2.7 | RNA sequencing (RNA-seq) and analysis

The tissue around lateral ventricle of rats from both the kaolin-induced hydrocephalus with 60 μL and control groups were isolated on ice, rapidly immersed in liquid nitrogen, and subsequently stored at −80°C.

Total RNA was isolated using the Trizol Reagent (Invitrogen Life Technologies) and its concentration, quality, and integrity were assessed with a NanoDrop spectrophotometer (Thermo Scientific). Using three micrograms of RNA for each sample, sequencing libraries were prepared as follows: mRNA was purified from the total RNA via poly-T oligo-attached magnetic beads. The mRNA was then fragmented using divalent cations at high temperature in a fragmentation buffer specific to Illumina. Synthesis of the first strand cDNA was performed using random oligonucleotides and SuperScript II, followed by second strand cDNA synthesis with DNA Polymerase I and RNase H. Remaining overhangs were converted into blunt ends via exonuclease/polymerase activities, and the enzymes were removed. The DNA fragments then had their 3′ ends adenylated, followed by ligation with Illumina PE adapter oligonucleotides for hybridization preparation. To select cDNA fragments of the preferred 400–500 bp in length, the library fragments were purified using the AMPure XP system (Beckman Coulter, Beverly, CA, USA). DNA fragments with ligated adaptor molecules on both ends were selectively enriched using Illumina PCR Primer Cocktail in a 15 cycle PCR reaction, purified with the AMPure XP system, and quantified on an Agilent Bioanalyzer 2100 system using a high sensitivity DNA assay (Agilent). Finally, the sequencing library was

sequenced on NovaSeq 6000 platform (Illumina) Shanghai Personal Biotechnology Cp., Ltd.

CSF data from human NPH patients and normal controls were publicly available and obtained from the Gene Expression Omnibus (GEO) database under accession number GSE212236, https://www.ncbi.nlm.nih.gov/geo/query/acc.cgi?acc=GSE212236,[23] and GSE189919, https://www.ncbi.nlm.nih.gov/geo/query/acc.cgi?acc=GSE189919,[24] respectively.

The R/Bioconductor package "DESeq2" was utilized to identify differentially expressed genes (DEGs) between the corresponding hydrocephalus group and control group. Genes with log2-fold change ≥1 and $p \leq 0.05$ were considered upregulated DEGs. Principal component analysis (PCA) was performed on the variance-stabilized transformation (VST) of read count values from NPH patients, hydrocephalus rats, and their respective control groups. The upregulated DEGs were subjected to Kyoto Encyclopedia of Genes and Genomes (KEGG) enrichment and Gene Ontology (GO) analysis using R clusterProfiler package, with visualization using R ggplot2 package. A bubble plot of significant co-enriched pathways ($p \leq 0.05$) in KEGG and GO analysis in human NPH patients and hydrocephalus rats was generated using the R ggplot2 package. The R pheatmap package was used to visualize the DEGs. The volcano plot was generated by R ggplot2 package.[7] The chord diagrams for KEGG and GO enrichment analyses of gene sets were drawn using the R circlize package.

2.8 | Statistical analysis

Statistical analysis was performed using SPSS 27.0 (IBM, Armonk, New York, NY, USA) and the data were described using means and standard deviations (SD). For data with normal distribution, paired *t*-test was used for intra-group comparisons, otherwise paired samples Wilcoxon signed rank test was used. For repeated time point measurements, such as body weight, indicators of the open field, new object recognition and Y-maze, repeated measures ANOVA were used to assess for analysis. The correlation between Evans index and body weight was calculated by Spearman correlation coefficient. The Evans index in the first and fourth month after kaolin injection was compared by two-way ANOVA. $p < 0.05$ was considered significant.

3 | RESULTS

Twenty-two rats were finally included in the analysis. The 200-day survival curves after kaolin injection of each group indicated that higher volume would decrease the survival length of the rats, as shown in Figure S2.

3.1 | Behavior assessment

3.1.1 | Anxiety level and motor ability

The results of open field test at the 7th week post kaolin injection are shown in Figure 2A. The statistical analysis demonstrated that the severity of induced hydrocephalus, reflected by anxiety level (Figure 2B) and motor ability (Figure 2C), is closely associated with injected volumes. The control group showed the most active behavior, while the kaolin-60 μL group showed the worst anxiety level ($p = 0.027$) and motor ability ($p = 0.005$).

3.1.2 | Recognition levels

In the new object recognition experiment, the control group spends longer time in exploring the new object, compared with the hydrocephalus group, especially the kaolin-60 μL group (Figure 2D,E). The recognition level of hydrocephalus rats, for example, kaolin-60 μL group deteriorates along time.

In the Y-maze spontaneous alternation experiment, no interaction effect exists between group and time, and there was no significant difference in spatial recognition ability among the four groups of rats (Figure S3).

3.2 | Body weight

Figure 3C shows that hydrocephalus has a significant influence on body weight development. In control group, the body weight gradually increases along time, however, in kaolin-60 μL and kaolin-90 μL groups, the body weight growth ceased (Figure 3C).

3.3 | MRI

T2-weighted MRI showed larger volumes of kaolin injection is positively related with larger ventricular size, with kaolin-60 μL group having the largest Evans index (Figure 3A). The result also demonstrated progressively expanded ventricles over time in the hydrocephalus groups compared to the control group (Figure 3B). 87.5% (14/16) of the rats in the kaolin injection groups showed enlarged ventricles in the first month, and the number of hydrocephalus rats increased to 93.75% (15/16) in the

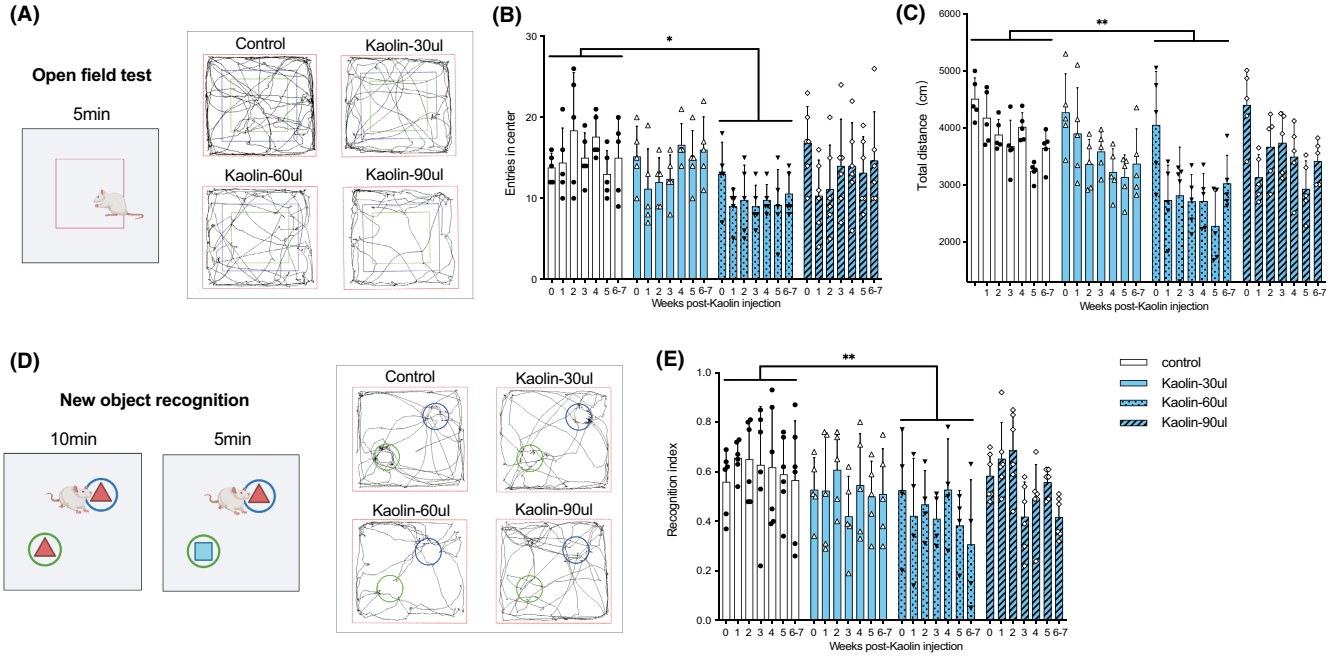

FIGURE 2 Effect of different volumes of kaolin injection on the behavior tests in rats. (A) The representative trace of each group of open field test at the 7th week after kaolin injection. The red box of the trace map showed the whole open field area, and the green box represented the central area. (B) Anxiety level was assessed by the entries in the center of the open field, which is closely associated with injected volume. The control group showed the most active behavior, while the kaolin-60 μL group showed the worst anxiety level. (C) Motor ability was assessed by total distance, which showed reduced movement in kaolin injection group, especially the kaolin-60 μL group. *: $P < 0.05$, **: $P < 0.01$; $n = 5$-6/group. Bar graphs represent mean ± SD. (D) The representative trace of each group of new object recognition test at the 7th week after kaolin injection. The green circle in the lower left corner is the location of the new object placement, and the blue circle in the upper right corner referred to the old object. (E) Cognitive memory ability was assessed by recognition index. The control group spends longer time in exploring the new object, compared with the hydrocephalus group, especially the kaolin-60 μL group. **: $P < 0.01$, $n = 4$-6/group. Bar graphs represent mean ± SD.

fourth month. Meanwhile, the study showed a negative relationship between the body weight and Evans index ($r = -0.514$, $p < 0.01$, Figure 3D).

The brain tissue showed kaolin mainly deposited in the bilateral subarachnoid space and the surface of the cerebellum (Figure 4A). Coronal T2-weighted MRI images showed the presence of kaolin deposits in the quadrigeminal cistern and the supracerebellar cistern in kaolin injection group. Hydrocephalus groups demonstrated ventricular enlargement, with the cerebral aqueduct remaining predominantly unobstructed and the basal cistern remaining open (Figure 4B).

3.4 | Histological evaluation

HE staining was used to examine the damage of the ependymal cells of the ventricles and inflammatory infiltrate of the hydrocephalus brain. The results showed that kaolin-induced hydrocephalus can lead to immune inflammatory response and the severity of inflammatory response was related with the volumes of kaolin injection (Figure 5A). In terms of the structure, kaolin-60 μL and kaolin-90 μL groups showed higher-grade inflammatory infiltrate and the damage of the structure of ependymal layer of the ventricles (Figure 5B).

3.5 | RNA-seq analysis

We conducted RNA-seq analyses of tissue around lateral ventricle from kaolin-induced hydrocephalus with 60 μL and control rats using NGS to measure RNA-seq. And we collected RNA-seq data of CSF from NPH patients from the GEO database and performed a comparative analysis with RNA-seq data from the rat hydrocephalus model. By integrating these data, we aim to elucidate the mechanisms and potential discrepancies in how the rat hydrocephalus model simulates human NPH disease.

PCA revealed distinct clustering in NPH patients and their control group, as well as in hydrocephalus rats and their control group. In NPH patients, the first principal component (PC1) and the second principal component

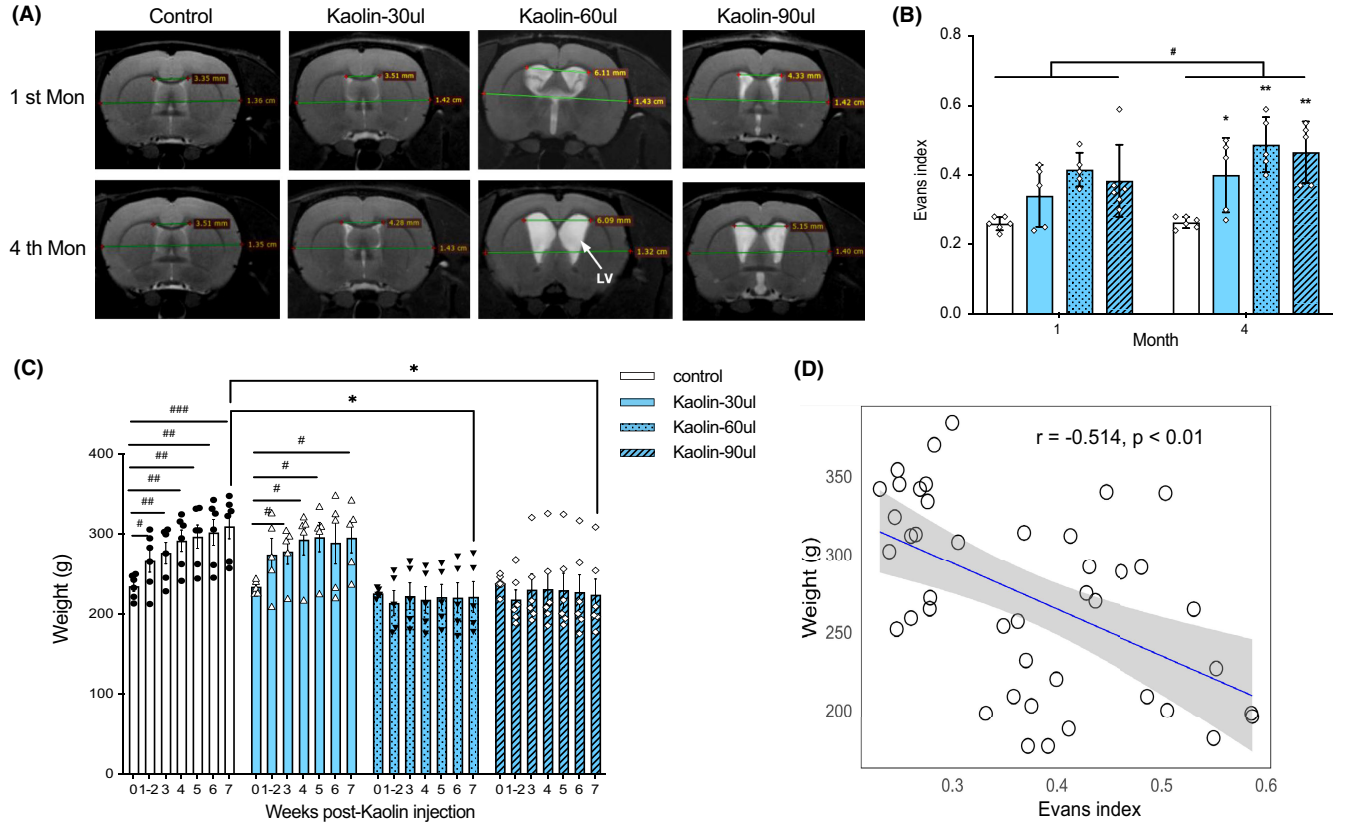

FIGURE 3 MRI for each group in the first and fourth months and the relationship between the Evans index and body weight in different kaolin injection groups. (A) Representative MRI images showed that the ventricles of the rats in the kaolin-30 μL, kaolin-60 μL group and kaolin-90 μL group increased over time. The Evans index was calculated as the ratio of the maximum width of the anterior horn of the lateral ventricle (upper green line) to the maximum width of the cranial cavity within the same dimension (bottom green line). LV — lateral ventricle. MRI — magnetic resonance imaging. (B) Evans index in rats with different kaolin injections at the first and fourth months. Evans index showed progressively expanded ventricles over time in the hydrocephalus groups compared to the control group. *: $P < 0.05$ vs. the control group, **: $P < 0.01$ vs. the control group; #: $P < 0.05$ vs. the first month, n = 5-6/group. Bar graphs represent mean ± SD. (C) Compared with week 0, the weight of control rats increased steadily with time in control group. In kaolin-60 μL and kaolin-90 μL groups, the body weight growth ceased. #: $P < 0.05$, ##: $P < 0.01$, ###: $P < 0.001$, *: $P < 0.05$, n = 5-6/group. Bar graphs represent mean ± SD. (D) Scatter plot of Evans index and body weight. Body weight of rats was negatively correlated with Evans index. r = −0.514, $p < 0.01$.

(PC2) accounted for 43.58% and 5.89% of the total variance (Figure 6A). In hydrocephalus rats, PC1 and PC2 accounted for 67.20% and 9.50% of the total variance (Figure 6B). 7970 DEGs (adjusted $p < 0.05$, 302 up and 7668 down) in NPH group, compared to the control people (Figure 6C,D), and 2202 DEGs (adjusted $p < 0.05$, 1830 up and 372 down) in hydrocephalus group compared to the normal rats (Figure 6E,F).

To investigate how the rat hydrocephalus model simulates human NPH disease, we screened for commonly downregulated differentially expressed genes and analyzed their known and predicted protein interaction networks. The results showed that in the STRING protein interaction network, *k*-means clustering analysis indicated that these genes were primarily concentrated in immune and inflammatory pathways (Figure 7A). Further analysis revealed that the central regulatory proteins of these genes included CD44, ICAM1, CXCL10, and CD40, which are associated with immune cells, cell adhesion, and immune and inflammatory responses (Figure 7B). KEGG and GO analyses were conducted on the commonly downregulated differentially expressed genes in hydrocephalus rats and NPH patients (Figure 7C–F).

KEGG enrichment analysis identified a significant abundance of key pathways in hydrocephalus rats associated with immune system, signal transduction, infectious disease, cell growth and death, and cardiovascular disease. Particularly, inflammatory pathways such as the Leukocyte transendothelial migration, C-type lectin receptor signaling pathway, Rap1 signaling pathway, JAK–STAT signaling pathway, and HIF-1 signaling pathway were prominent in hydrocephalus rats, resembling the conditions in human NPH patients (Figure 8A,B).

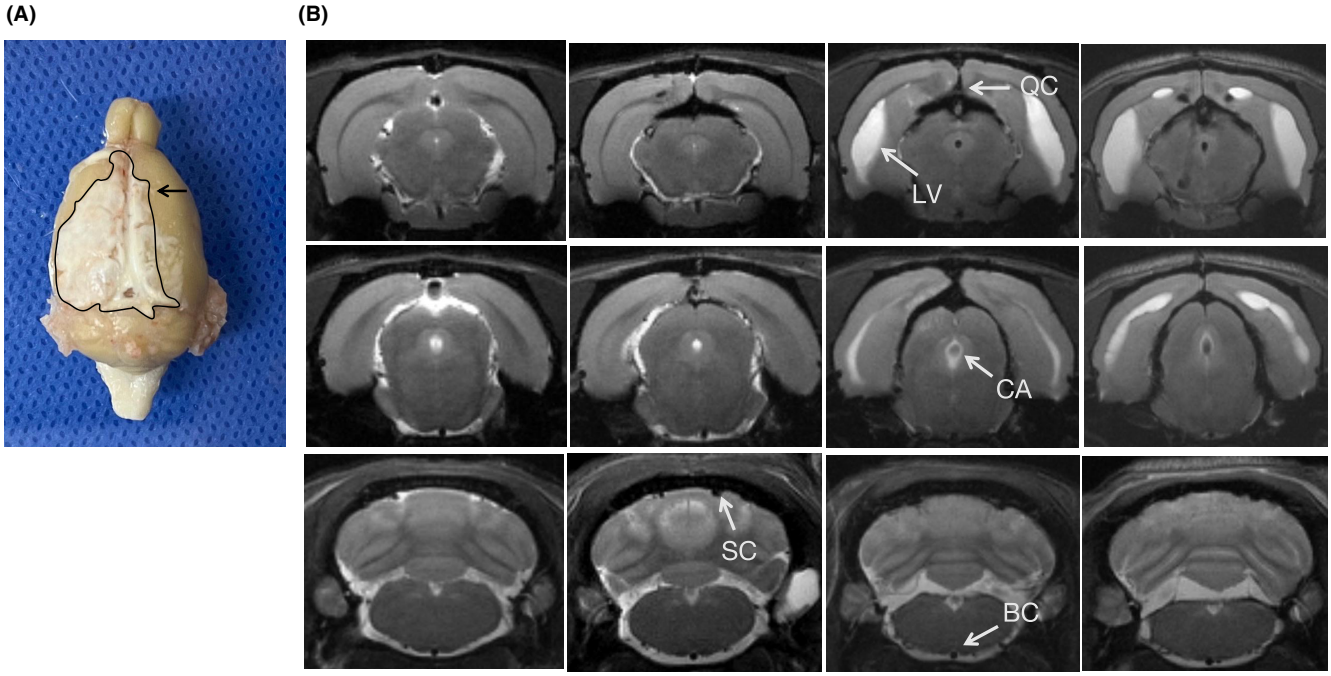

FIGURE 4 Post injection distribution of kaolin extension. (A) Typical characteristics of kaolin deposits in the subarachnoid space above the brain. Kaolin was observed at the cortical convexities and in close proximity to the superior sagittal sinus, extending to the surface of the cerebellum. Arrow: Range of kaolin deposits. (B) Representative coronal T2-weighted MRI images of rats with different kaolin injections at the fourth month. In the groups exposed to kaolin, the presence of kaolin deposits was observed in both the quadrigeminal cistern and the supracerebellar cistern. Hydrocephalus groups demonstrated ventricular enlargement, with the cerebral aqueduct remaining predominantly unobstructed and the basal cistern remaining open. QC—Quadrigeminal cistern, LV—Lateral ventricle, CA—Cerebral aqueduct, SC—Supracerebellar cistern, BC—Basal cistern.

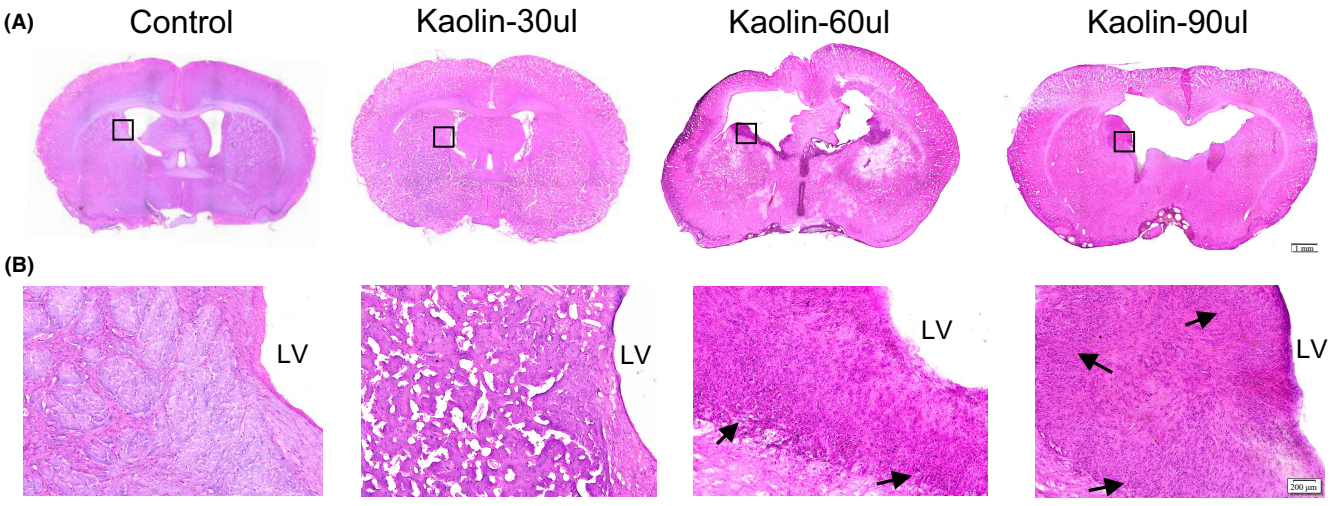

FIGURE 5 HE staining of sections from lateral ventricles of rats injected with different volumes of kaolin. (A) Representative full-scans of rats' lateral ventricles for the control, kaolin-30 μL, kaolin-60 μL, and kaolin-90 μL groups. The severity of inflammatory response was related with the volumes of kaolin injection. (B) Representative enlarged views of rats' lateral ventricles for the control and hydrocephalus groups. Kaolin-60 μL and kaolin-90 μL groups showed higher-grade inflammatory infiltrate and the damage of the structure of ependymal layer of the ventricles. Black arrow: Inflammatory infiltrate. Scale bars, 1 mm (A), 200 μm (B).

In the cellular component (CC) aspect of GO, the results for the rat hydrocephalus model and NPH patients showed a similar trend to the KEGG analysis. These enriched processes indicate that in the hydrocephalus model and NPH patients, apoptotic cells and immune cells related to immune inflammation play important roles in regulating

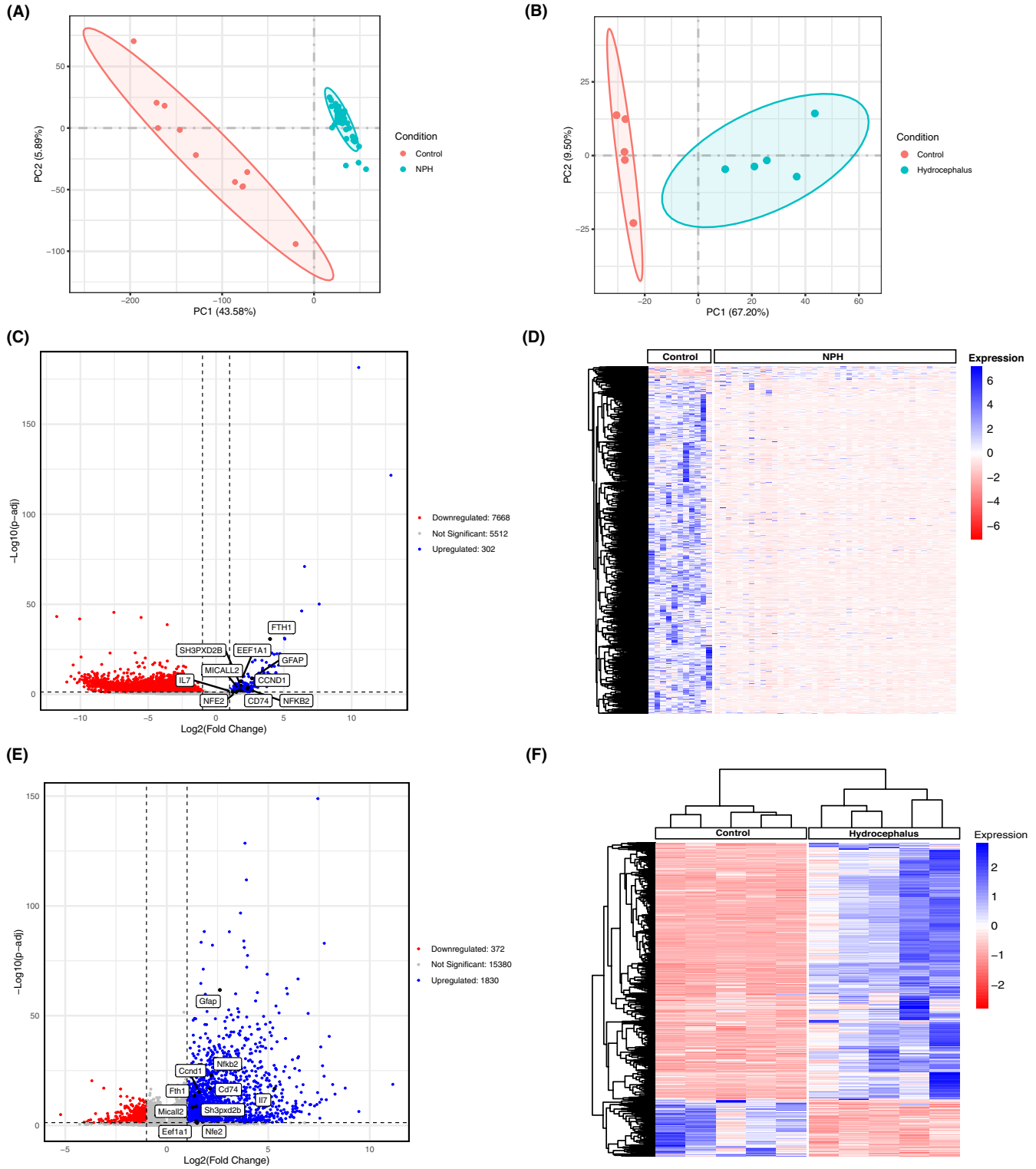

FIGURE 6 PCA scores and visualization of DEGs in NPH patients and hydrocephalus rats. (A) Plot of PCA scores in NPH patients and normal controls. (B) Plot of PCA scores in hydrocephalus rats and control group. (C) Volcano plot of DEGs in NPH patients and normal controls. (D) The heatmap displays DEGs between NPH patients and normal controls. Red and blue colors indicate DEGs by upregulated and downregulated, respectively. (E) Volcano plot of DEGs in hydrocephalus rats and control group. (F) The heatmap of DEGs between hydrocephalus rats and control group.

and participating in these biological processes. Specifically, these results are mainly enriched in the following biological processes: negative regulation of apoptotic signaling pathway, negative regulation of intrinsic apoptotic signaling pathway, positive regulation of B-cell proliferation, regulation of apoptotic signaling pathway, regulation of

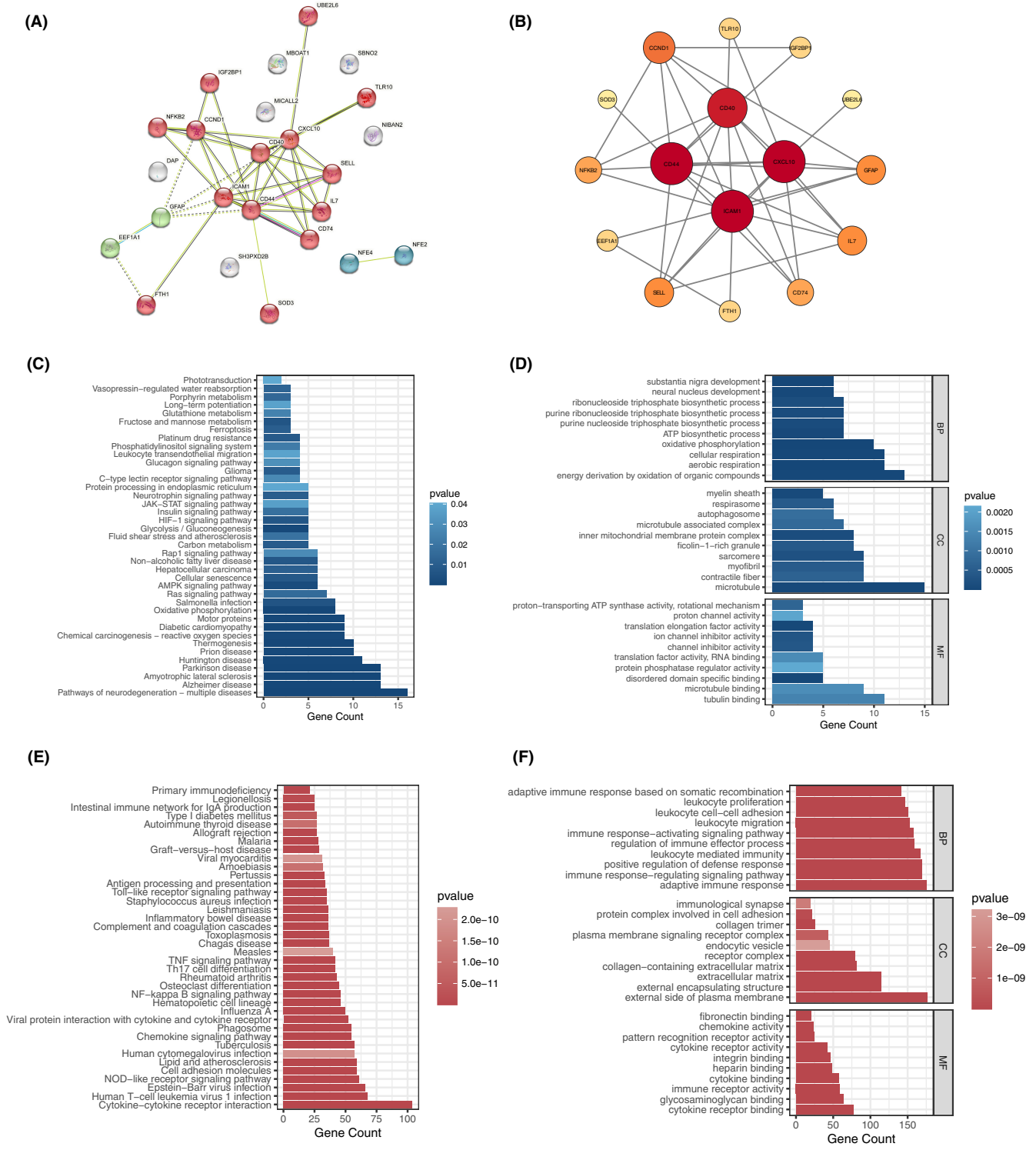

FIGURE 7 Analysis of commonly up-regulated DEGs and KEGG/GO analyses in NPH patients and hydrocephalus Rats. (A) Clustering of commonly up-regulated DEGs using STRING network analysis. (B) Utilizing Cytoscape for the analysis of commonly up-regulated DEGs. (C) KEGG analysis of up-regulated DEGs in NPH patients and normal controls. (D) GO analysis of up-regulated DEGs in NPH patients and normal controls. (E) KEGG analysis of up-regulated DEGs in hydrocephalus rats and control group. (F) GO analysis of up-regulated DEGs in hydrocephalus rats and control group.

B-cell proliferation, regulation of intrinsic apoptotic signaling pathway, and regulation of leukocyte proliferation (Figure 8C,D). Overall, these findings reveal the crucial role of apoptosis and immune-inflammatory responses in the progression of hydrocephalus and NPH, suggesting that these pathways could be potential therapeutic targets.

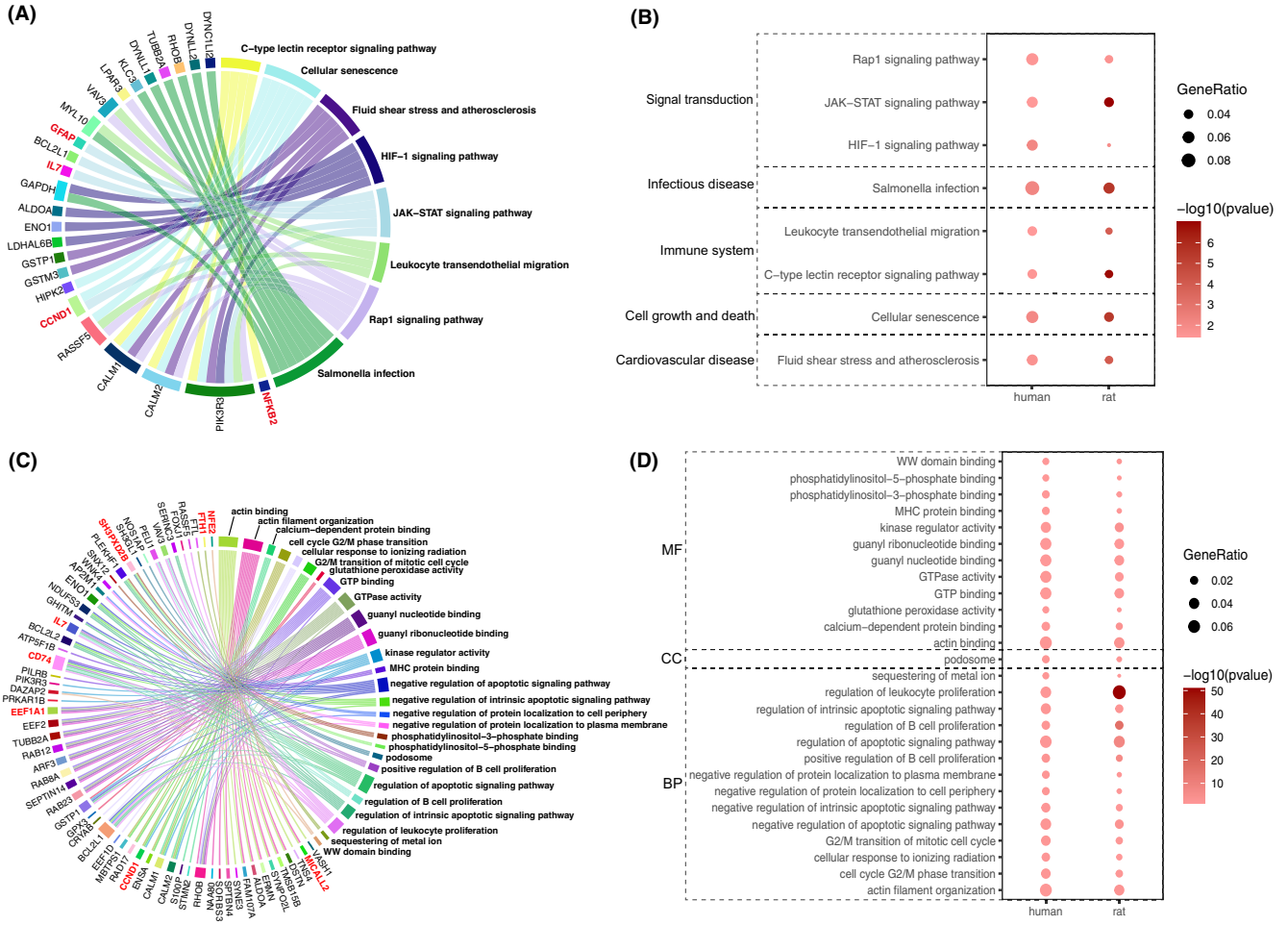

FIGURE 8 The transcriptome of hydrocephalus rats and comparison with human NPH patients. (A, B) Chord diagram and bubble plot of co-enriched KEGG pathway analysis showed a significant enrichment of pivotal pathways involved in immune system, signal transduction, infectious disease, cell growth and death, and cardiovascular disease. DEGS in co-enriched KEGG pathways were marked in red. (C, D) Chord diagram and bubble plot of co-enriched GO pathway analysis. DEGS in co-enriched GO pathways were marked in red.

4 | DISCUSSION

Hydrocephalus is a common disease in children and elder people which causes a big burden to the society due to its life-threatening complications. Currently, the most effective treatment is shunt surgery, which is prone to malfunction, obstruction, and infection. Moreover, there is no effective pharmacological treatment for hydrocephalus yet.[7,25] An effective animal model plays a vital role in understanding the disease and inspiring new treatments.

A variety of hydrocephalus models have been developed by injecting different materials into the brain. Cherian et al.[26] induced hydrocephalus model by injecting blood in the lateral ventricle. Hydrocephalus model after subarachnoid hemorrhage was induced by injecting blood in cisterna magna, with high mortality.[27] Dandy et al.[28,29] induced obstructive hydrocephalus by placing cotton in a gelatin capsule and pushing it into the aqueduct of Sylviu in dogs. Del Bigio et al.[30] induced hydrocephalus by injecting silicone oil into the cisterna magna of adult rabbits, which only represents short-term pathological changes of hydrocephalus. However, the current animal models of hydrocephalus is not able to simulate real symptoms of the disease, either because of high mortality, or due to different progressive speed compared with humans.[30]

Kaolin injection induced hydrocephalus have been widely used as a mature animal model[31,32]; however, we still lack a standard strategy for unified model establishment which might introduce variance in further studies. Moreover, the influence of different volumes injection in animal behavior and ventricular size needs further investigation. To simulate NPH in humans, we selected 2-month-old adult rats for the experiment. We continuously observed behavioral manifestations for nearly 2 months and assessed imaging characteristics for up to 4 months following the induction of hydrocephalus. In the current study, we tested the severity of hydrocephalus

at different volumes of kaolin injection. Both the body weight, anxiety level, recognition ability and motor ability declined significantly with increase injection volumes. We also conducted the grip experiment, with both kaolin-60 μL and kaolin-90 μL groups showing a noticeable weak grip compared to control group (Figure S4). The histological analysis indicates obvious inflammatory response in kaolin-60 μL group and kaolin-90 μL group. Patients with hydrocephalus often suffer with gait abnormalities, which was also validated in our study by decreased step rate and walking speed in the hydrocephalus rat group (Figure S5a,b), with kaolin-60 μL group showing the biggest effect.

Evans Index calculated from MRI imaging was used to assess the successful rate of the model. The result showed highest successful rate in the kaolin-60 μL group within 1 month after kaolin injection, that is, 100% successful rate. The mortality was influenced by different volumes, with two rats who representing the largest Evans index from the kaolin-90 μL group and the preexperimental 120 μL group died rats 1 month after kaolin injection, possibly due to an overdose (Figure S1). Other modeled rats survived longer than 7 months.

In clinical practice, patients with hydrocephalus always suffer from cognitive deficits and physical disability. However, some patients do not show functional impairment, despite severe abnormalities in brain structure.[33] Similar findings were also presented in a 2-year-old rat named R222, who lived with normal motor function, even with severe hydrocephalus.[34] The description above may be the reason why the kaolin-90 μL group's performance relatively normal. The exact reason still needs further investigation.

In our animal model, the HE staining result indicates that inflammation plays a critical role in the pathogenesis of hydrocephalus, which matches with previous findings. Karimy et al.[35] established a rat model of post-hemorrhagic hydrocephalus (PHH). This was achieved by intracerebroventricular injection of sterile autologous blood into male Wistar rats that were 8 weeks old. The authors demonstrated that intraventricular hemorrhage (IVH) induces the activation of Toll-like receptor 4 (TLR4) and nuclear factor kappa B (NF-κB)-dependent inflammatory responses in choroid plexus epithelial cells, which are associated with increased CSF secretion. Robert et al.[7] found that infectious hydrocephalus (PIH) and PHH exhibit strikingly similar immune and secretory responses at the choroid plexus, which contribute to the abnormal secretion of CSF. Zhu et al.[36] conducted an experiment in which they administered kaolin into the cisterna magna of C57BL/6 mice to induce hydrocephalus. They have demonstrated that activated microglia are associated with ventricular expansion and behavioral abnormalities. In summary, neuroinflammation might be a critical factor in hydrocephalus, however, further investigations need to be done for the next step to clarify which is the main pathologic reason of hydrocephalus symptoms, the inflammatory response, or the blockage of CSF circulation.

Chen et al.[37] compared the transcriptomic alterations in lung tissues across various animal models with COVID-19 patients. They discovered significant enrichment of key pathways associated with innate immune responses, inflammation, cytokine-cytokine receptor interactions, chemokine, and adhesion pathways among human COVID-19 patients and multiple animal models. In our research, we also identified co-enriched pathways between the model outlined in this paper and human NPH patients from public database by transcriptomics analysis. The rat model of hydrocephalus induced by kaolin injection into the subarachnoid space was able to resemble the inflammatory mechanism observed in human NPH patients according to the co-enrichment pathway analysis in KEGG analysis, which was also consistent with our histopathological examination results.

Although the kaolin method is widely used and relatively simple to operate, kaolin-induced hydrocephalus may not accurately represent the pathophysiology of human chronic hydrocephalus. In this study, we compared data from publicly available databases of NPH patients with our animal model. The analysis indicated that this model effectively simulates immune-inflammatory mechanisms related to genes such as CD40, CD44, CXCL10, and ICAM. However, the etiology of human hydrocephalus is complex, and this model cannot fully replicate the pathophysiology of human hydrocephalus. We chose bilateral subarachnoid space as the injection site, and our experiments revealed that the site and volume of kaolin injection significantly influence the severity of hydrocephalus, leading to variable animal behavior. Moreover, this study only examined the response of rats to kaolin, and there may be species-specific differences that warrant further investigation.

Numerous animal models of hydrocephalus have been developed. To fully understand the utility of the models, continual comparison with human diseases is essential. The utilization of parallel multi-omics data from humans might be used to better understand at a systems level how well the model phenocopies the human disease.[37] Thorough analysis is pivotal for refining model selection criteria and interpreting results, thereby advancing our further understanding of the pathophysiological mechanisms underlying hydrocephalus.[38]

This study summarizes the characterization of kaolin-induced hydrocephalus with different injection volumes. The severity and pathological symptoms are closely associated with injection volumes, with higher volumes

resulting in deterioration of behavior and weight loss. 60 μL injection might be recommended for the establishment of hydrocephalus animal model, with a high successful rate and high stability, and the rats with hydrocephalus were able to resemble the inflammatory mechanism and behavioral performance observed in human NPH patients. The model holds promise for investigations and new treatments development of hydrocephalus in the future.

AUTHOR CONTRIBUTIONS

All authors designed the experiments. Zhang Kuo, Wanqi Zhou, Huijie Yu, Huixin Gao and Faheem Anwar performed the experiment. Zhang Kuo, Wanqi Zhou and Meijun Pang analyzed and interpreted the data. Zhang Kuo and Wanqi Zhou drafted the work. Xiuyun Liu and Dong Ming revised the manuscript critically for important intellectual content. All authors have read and approved the final submitted manuscript. All authors are agreed to be accountable for all aspects of the work.

ACKNOWLEDGMENTS

This work was supported by National Key R&D Program of China (2021YFF1200602), National Science Fund for Excellent Overseas Scholars (0401260011), National defense science and technology innovation project (c02022088), Tianjin University Independent Innovation Fund (2023XYY-0042), and China Postdoctoral Science Foundation (2020T130092ZX).

CONFLICT OF INTEREST STATEMENT

The authors declare they have no conflicts of interest.

DATA AVAILABILITY STATEMENT

The data that support the findings of this study are available from corresponding author upon reasonable request. Data from human NPH patients and normal controls that supports the findings of this study are available in the GEO database, accession number GSE212236, https://www.ncbi.nlm.nih.gov/geo/query/acc.cgi?acc=GSE212236, and GSE189919, https://www.ncbi.nlm.nih.gov/geo/query/acc.cgi?acc=GSE189919, respectively.

ETHICS STATEMENT

The hydrocephalus model used in these studies was female Sprague–Dawley rats. All the procedures followed the International Guide for the Care and Use of Laboratory Animals and were approved by the Animal Ethics Committee of Tianjin University in China (No. TJUE-2023–070).

ORCID

Xiuyun Liu https://orcid.org/0000-0001-9540-4865

REFERENCES

1. Edwards RJ, Dombrowski SM, Luciano MG, Pople IK. Chronic hydrocephalus in adults. *Brain Pathol*. 2004;14:325-336.
2. Isaacs AM, Riva-Cambrin J, Yavin D, et al. Age-specific global epidemiology of hydrocephalus: systematic review, metanalysis and global birth surveillance. *PLoS One*. 2018;13:e0204926.
3. Vinchon M, Rekate H, Kulkarni AV. Pediatric hydrocephalus outcomes: a review. *Fluids Barriers CNS*. 2012;9:1-10.
4. Simon TD, Riva-Cambrin J, Srivastava R, Bratton SL, Dean JM, Kestle JR. Hospital care for children with hydrocephalus in the United States: utilization, charges, comorbidities, and deaths. *J Neurosurg*. 2008;1:131-137.
5. Kahle KT, Kulkarni AV, Limbrick DD, Warf BC. Hydrocephalus in children. *Lancet*. 2016;387:788-799.
6. Anderson IAS. Factors associated with 30-day ventriculoperitoneal shunt failure in pediatric and adult patients. *J Neurosurg*. 2019;130:145-153.
7. Robert SM, Reeves BC, Kiziltug E, et al. The choroid plexus links innate immunity to CSF dysregulation in hydrocephalus. *Cell*. 2023;186(764–785):e21.
8. Davis LE. Communicating hydrocephalus in newborn hamsters and cats following vaccinia virus infection. *J Neurosurg*. 1981;54:767-772.
9. Fiori MG, Sharer LR, Lowndes HE. Communicating hydrocephalus in rodents treated with β, β'-iminodipropionitrile (IDPN). *Acta Neuropathol*. 1985;65:209-216.
10. Moinuddin SM, Tada T. Study of cerebrospinal fluid flow dynamics in TGF-β1 induced chronic hydrocephalic mice. *Neurol Res*. 2000;22:215-222.
11. Wiesmann M, Koedel U, Brückmann H, Pfister HW. Experimental bacterial meningitis in rats: demonstration of hydrocephalus and meningeal enhancement by magnetic resonance imaging. *Neurol Res*. 2002;24:307-310.
12. Borit A, Sidman RL. New mutant mouse with communicating hydrocephalus and secondary aqueductal stenosis. *Acta Neuropathol*. 1972;21:316-331.
13. Dahme M, Bartsch U, Martini R, Anliker B, Schachner M, Mantei N. Disruption of the mouse L1 gene leads to malformations of the nervous system. *Nat Genet*. 1997;17:346-349.
14. Del Bigio MR, Wilson MJ, Enno T. Chronic hydrocephalus in rats and humans: white matter loss and behavior changes. *Ann Neurol*. 2003;53:337-346.
15. Khan OH, Enno TL, Del Bigio MR. Brain damage in neonatal rats following kaolin induction of hydrocephalus. *Exp Neurol*. 2006;200:311-320.
16. da Silva LL, Slobodian I, Del Bigio MR. Characterization of juvenile and young adult mice following induction of hydrocephalus with kaolin. *Exp Neurol*. 2009;219:187-196.
17. Feng Z, Tan Q, Tang J, et al. Intraventricular administration of urokinase as a novel therapeutic approach for communicating hydrocephalus. *Transl Res*. 2017;180(77–90):77.e2-90.e2.
18. Li J, McAllister JP II, Shen Y, et al. Communicating hydrocephalus in adult rats with kaolin obstruction of the basal cisterns or the cortical subarachnoid space. *Exp Neurol*. 2008;211:351-361.
19. Jusué-Torres I, Jeon LH, Sankey EW, et al. A novel experimental animal model of adult chronic hydrocephalus. *Neurosurgery*. 2016;79:746-756.
20. Davis CM, Zhang WH, Bah TM, et al. Age-dependent cognitive impairment, hydrocephalus and leukocyte infiltration in

transgenic mice with endothelial expression of human EPHX2. *NPJ Aging*. 2022;8:9.
21. Kim JO, Jung DY, Min BI. Avocado Peel extract: the effect of radiation-induced on neuroanatomical and behavioral changes in rats. *J Chem Neuroanat*. 2023;129:102240.
22. Romeiro TH, Da Silva SC, da Silva BP, et al. The association of Edaravone with shunt surgery improves behavioral performance, reduces astrocyte reaction and apoptosis, and promotes neuroprotection in young hydrocephalic rats. *J Chem Neuroanat*. 2022;119:102059.
23. Levin Z, Leary OP, Mora V, et al. Cerebrospinal fluid transcripts may predict shunt surgery responses in normal pressure hydrocephalus. *Brain*. 2023;146:3747-3759.
24. Lee B, Mahmud I, Pokhrel R, et al. Medulloblastoma cerebrospinal fluid reveals metabolites and lipids indicative of hypoxia and cancer-specific RNAs. *Acta Neuropathol Commun*. 2022;10:25.
25. Blazer-Yost BL. Consideration of kinase inhibitors for the treatment of hydrocephalus. *Int J Mol Sci*. 2023;24:6673.
26. Cherian S, Thoresen M, Silver IA, Whitelaw A, Love S. Transforming growth factor-βs in a rat model of neonatal posthaemorrhagic hydrocephalus. *Neuropathol Appl Neurobiol*. 2004;30:585-600.
27. Long C-Y, Huang G-Q, Du Q, Zhou L-Q, Zhou J-H. The dynamic expression of aquaporins 1 and 4 in rats with hydrocephalus induced by subarachnoid haemorrhage. *Folia Neuropathol*. 2019;57:182-195.
28. Dandy WE. Experimental hydrocephalus. *Ann Surg*. 1919;70:129-142.
29. Dandy WE, Blackfan KD. An experimental and clinical study of internal hydrocephalus. *JAMA*. 1913;61:2216-2217.
30. Del Bigio MR, Bruni JE. Silicone oil-induced hydrocephalus in the rabbit. *Childs Nerv Syst*. 1991;7:79-84.
31. Collins P. Experimental obstructive hydrocephalus in the rat: a scanning electron microscopic study. *Neuropathol Appl Neurobiol*. 1979;5:457-468.
32. Hochwald GM, Sahar A, Sadik AR, Ransohoff J. Cerebrospinal fluid production and histological observations in animals with experimental obstructive hydrocephalus. *Exp Neurol*. 1969;25:190-199.
33. Lewin R. Is your brain really necessary? John Lorber, a British neurologist, claims that some patients are more normal than would be inferred from their brain scans. *Science*. 1980;210:1232-1234.
34. Ferris CF, Cai X, Qiao J, et al. Life without a brain: Neuroradiological and behavioral evidence of neuroplasticity necessary to sustain brain function in the face of severe hydrocephalus. *Sci Rep*. 2019;9:1-10.
35. Karimy JK, Zhang J, Kurland DB, et al. Inflammation-dependent cerebrospinal fluid hypersecretion by the choroid plexus epithelium in posthemorrhagic hydrocephalus. *Nat Med*. 2017;23:997-1003.
36. Zhu J, Lee MJ, Chang HJ, et al. Reactive microglia and mitochondrial unfolded protein response following ventriculomegaly and behavior defects in kaolin-induced hydrocephalus. *BMB Rep*. 2022;55:181-186.
37. Chen Z, Yuan Y, Hu Q, et al. SARS-CoV-2 immunity in animal models. *Cell Mol Immunol*. 2024;21:119-133.
38. Dawson TM, Golde TE, lagier-Tourenne C. Animal models of neurodegenerative diseases. *Nat Neurosci*. 2018;21:1370-1379.

SUPPORTING INFORMATION

Additional supporting information can be found online in the Supporting Information section at the end of this article.

How to cite this article: Zhang K, Zhou W, Yu H, et al. Insights on pathophysiology of hydrocephalus rats induced by kaolin injection. *FASEB BioAdvances*. 2024;6:351-364. doi:10.1096/fba.2024-00070